Chapter 9

Pulse Current Auxiliary Sintering

Zhang Chunping and Zhang Kaifeng

Additional information is available at the end of the chapter

http://dx.doi.org/10.5772/53469

1. Introduction

1.1. Origin and development

Pulse current auxiliary sintering (PCAS) originated from electric current auxiliary sintering technique (ECAS), whose history can be traced back to the year of 1922, when an American did a path-breaking work to heat oxide powders by an electric current and synthesized a dense material. Then in 1927, another man sintered metal powders by simultaneously applying an electric current and a uniaxial mechanical load [1]. Since then, the synthesis technique has been being improved and perfected by numerous researchers. Up to now, over 1800 papers have been reported on the subject of ECAS and the technique has come to a new level: the used electric current extended from constant direct current to alternating current or pulsed electric current; power source was firstly selected to produce electric current, then capacitor banks were used; loading conditions evolved from no loading to uniaxial mechanical loaded or even multi-axial loading, etc.. Since 1960s, the technique commences to be commercialized. So far, it has been used to synthesize a large family of materials, including ceramics, intermetallics, metal-ceramic and ceramic-ceramic composites with various powders, such as elemental powders, pre-alloyed powders, pre-synthesized powders, or mechanical milled powders.

As a method to synthesize powers by applying electric current and mechanical loading simultaneously, ECAS technique revealed its increasing importance in the coming-out of a large amount of relevant bibliographies. Fig.1 shows the statistics of the number of articles on the subject published since the year 1922. It can be known that since 1999, the number of publications have been increased exponentially. If countries are weighed by the number of relevant articles, Japan, China and Korea are listed in the top three, as given in Fig. 2., while the contribution of other countries to the field remains relatively insignificant.

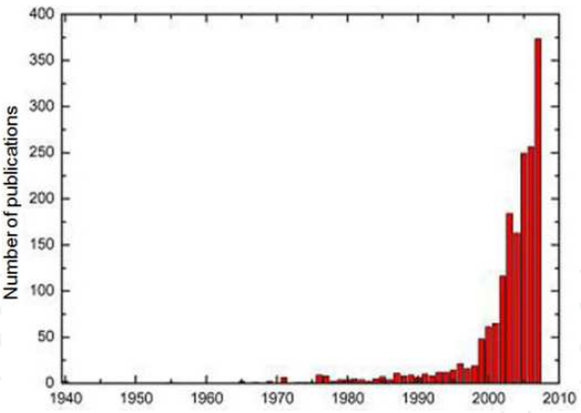

Figure 1. Number of publications related to ECAS processes by year [1]

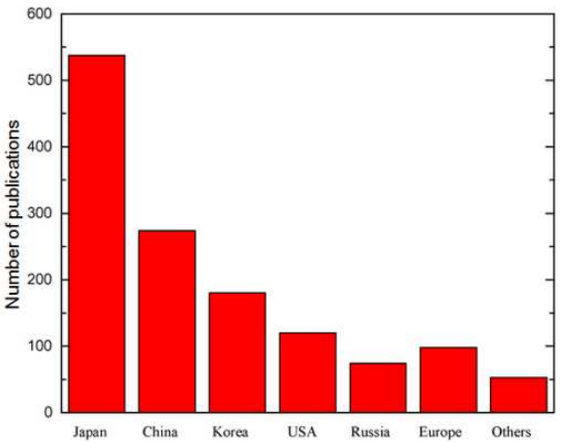

Figure 2. Publications related to ECAS numbered by country [1]

1.2. Classification

According to the standard classification in the sintering process, ECAS belongs to pressurized solid compaction [2], as drafted in Fig.3.

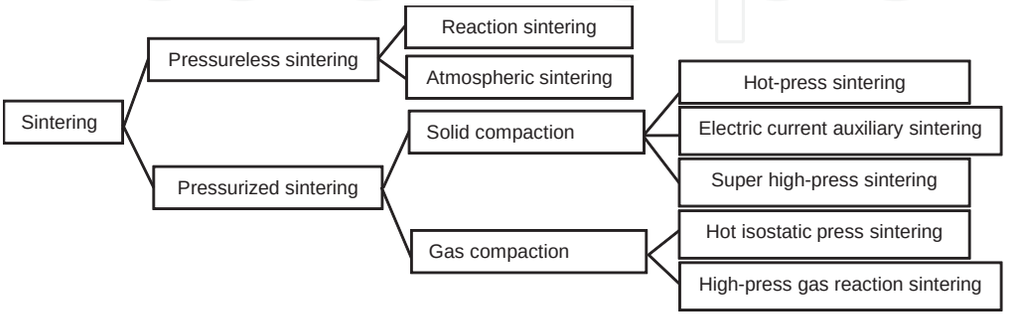

Figure 3. Standard classification of sintering process

http://dx.doi.org/10.5772/53469

When based on characteristics of the applied electric current, ECAS itself can be divided into two categories: Resistance Sintering (RS) and Electric Discharge Sintering (EDS) [3]. The former, RS, adopts direct current, alternating current or pulsed current with low voltage (dozens of volts) and high current (thousands of amperes) to sinter powders in action time ranging from 10^0s to 10^3s. In contrast, in EDs, powders were sintered by the electrical current with high voltage and high current from capacitor bank, in which abundant electrical energy is stored and can be launched instantaneously. But, most especially, the sintering process is often accompanied by electromagnetic phenomenon [4]. The distinction between the two categories has been listed in Table 1. Fig. 4 presents the statistics on the number of articles regarding the two categories of techniques [1]. As seen, studies on RS are far more numerous. The subject of this chapter, PCAS, is in the range of RS.

	Current origin	Current waveform	Voltage /current	Electromagnetic phenomenon	Action duration (s)
RS	power	constant direct current/ alternating pulsed current	low voltage high current	no	$10^0 \sim 10^3$
EDS	capacitor bank	large pulsed current	high voltage high current	yes	$10^{-5} \sim 10^{-3}$

Table 1. Differences between Resistance Sintering (RS) and Electric Discharge Sintering (EDS)

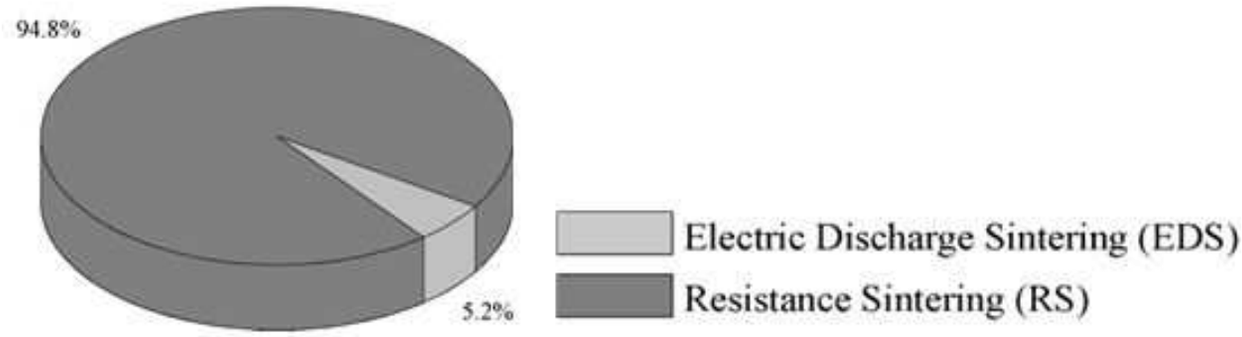

Figure 4. Relative amount of scientific reports regarding the two main ECAS processes

RS equipments used by researchers in different countries were purchased directly from commercial corporations, or developed by scientific institutions or researchers themselves for facilitate their own studies. Apart from the RS equipments developed by the two Japanese companies (Spark Plasma Sintering apparatus, well known as SPS), user-built machines accounts for about 40% among all the current RS machines, as introduced in Fig.5, where other companies refer to Sodick Co. Ltd [5]., Superior Graphite Co. Ltd.(USA) [6], Materials Modification Inc.(USA) [7], Eltek Co.(Korea) [8]etc.. All the user-built machines were named diversely to distinguish them from the commercial equipments. Fig. 6 shows a huge variety of RS designations. It is worth noting that almost all the names reflect the use of electric cur-

rent [9]. For example, plasma activated sintering (PAS), pulse current hot pressing (PCHP), and so on. In the lab where the author of the chapter works, a similar apparatus was also developed and named ZLY-60 Pulse Current Auxiliary Sintering (PCAS) to distinguish it from other used machines. The photo of the machine has been given in Fig.7. In RS, 4 electric current waveforms have been mentioned [10-18], as shown in Fig. 8. Among them, the third one, pulsed direct current, was the most common current. In PCAS, such a current was adopted for a series of studies.

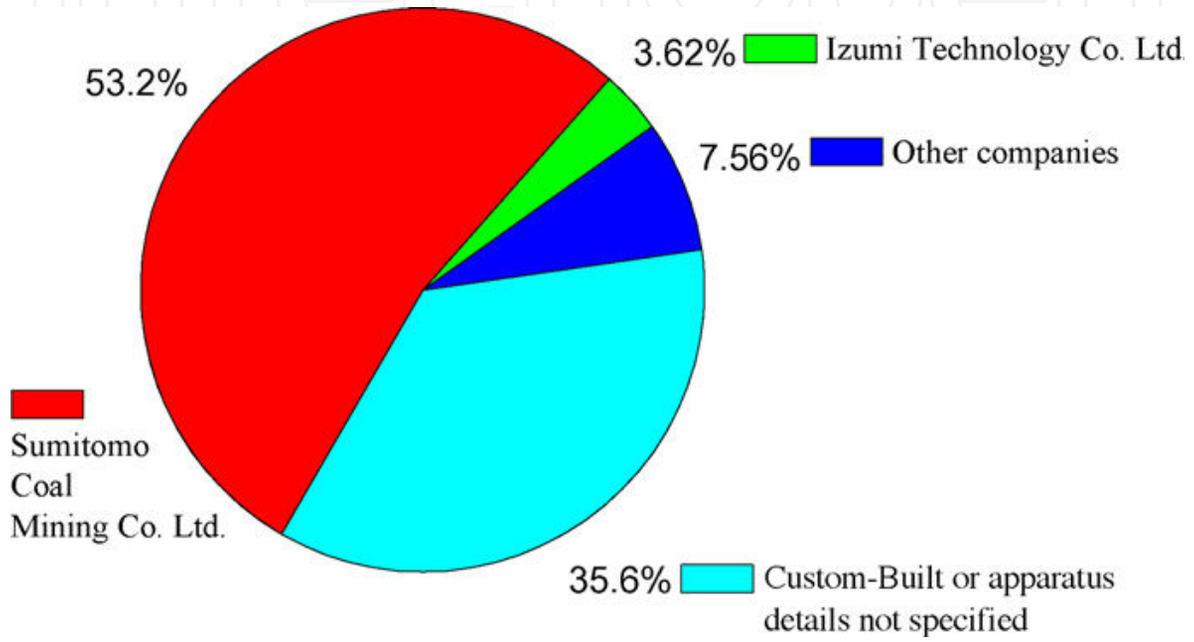

Figure 5. Relative distribution of apparatuses adopted in the RS processes as reported

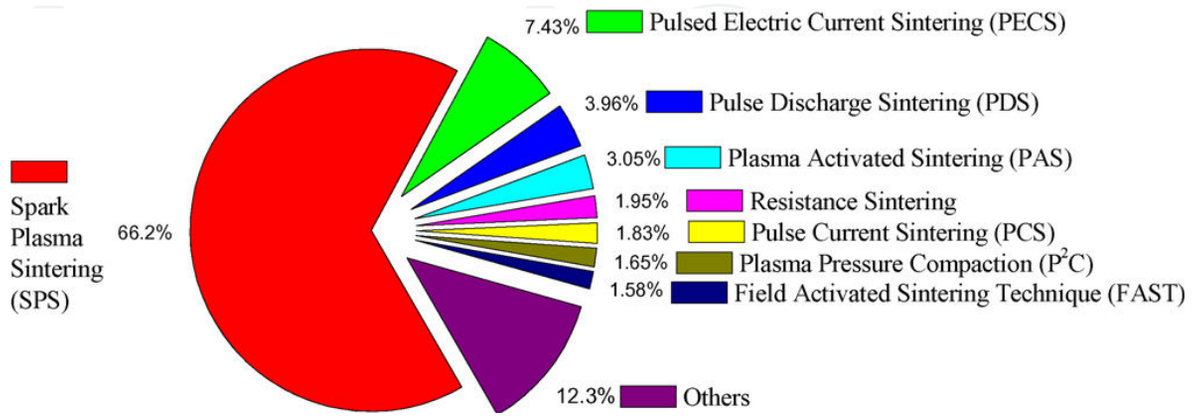

Figure 6. RS processes designation [1].

http://dx.doi.org/10.5772/53469

Figure 7. ZLY-60 pulse current auxiliary sintering apparatus

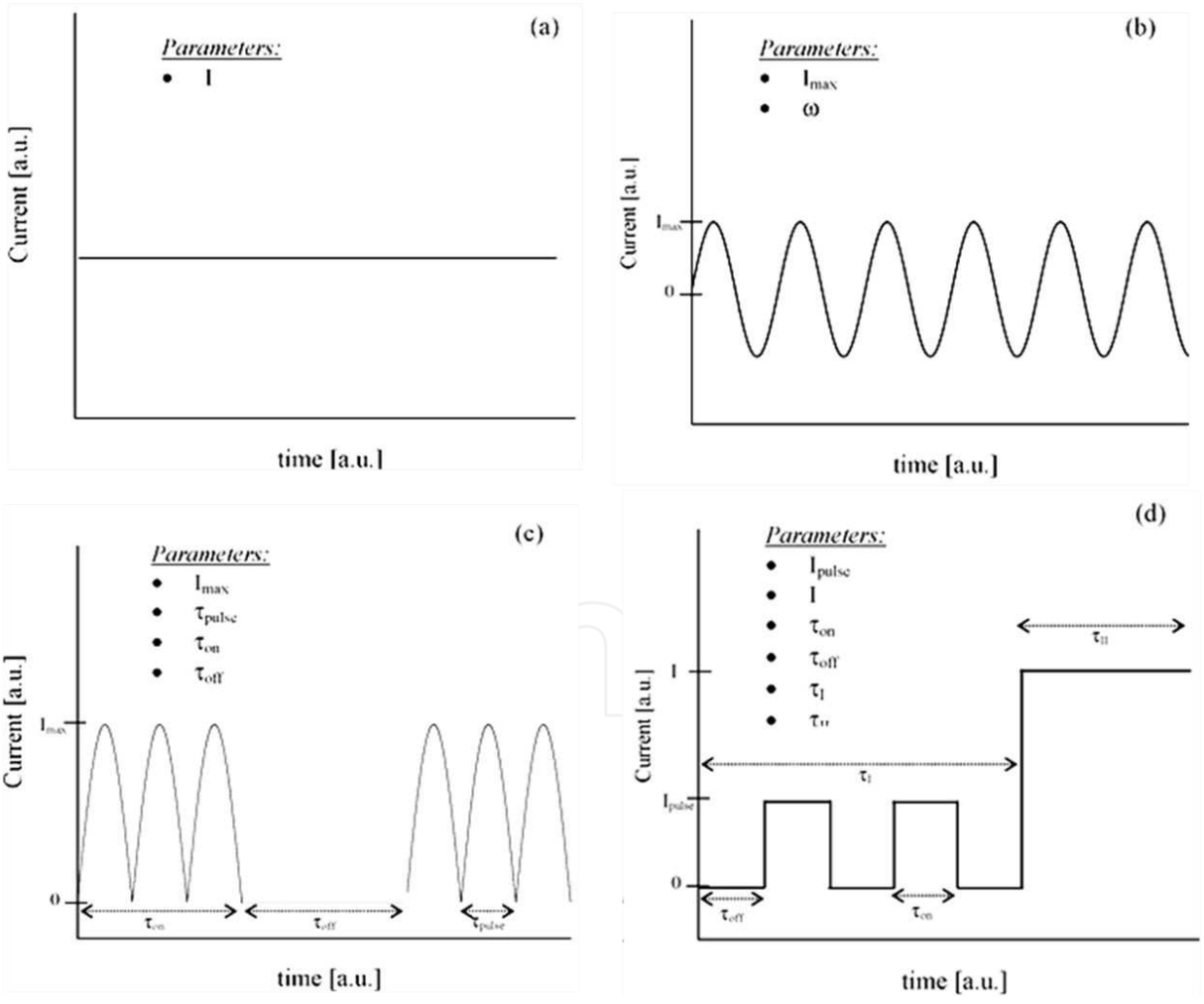

Figure 8. Typical electric current waveforms applied in the RS processes; (a) constant direct current (DC)(b) alternating current (AC) (c) pulsed direct current(d) pulsed direct current + direct current

1.3. Device structure and working fundamental mechanisms

PCAS equipment consists of three parts, as shown in Fig.9: (1) sintering mold and the device to provide an axial force, the force which can be adjusted in terms of synthesized material properties; (2) pulsed DC generator to generate electrical current to activate material powders; (3) electrical resistance heating part. When PCAS is in use, loose powders are firstly put into the die, then the furnace is vacuumed before the die is pressurized. In the sintering process, heat is provided by passing an electric current through the upper and lower punches, the powders and their container. Because of the multi-channel to transfer the current, the heat transfer rate is that high and the temperature can arrive at 1000~2000°C in a few seconds or minutes. What's more, heating rate and sintering temperature are both in control by adjusting the magnitude of pulsed current. Coupled with the load regulating system (the applied load can be quite low, say, 20~30MPa, or quite high, 500~1000MPa), PCAS can be utilized to synthesize metals, ceramics, and composite materials.

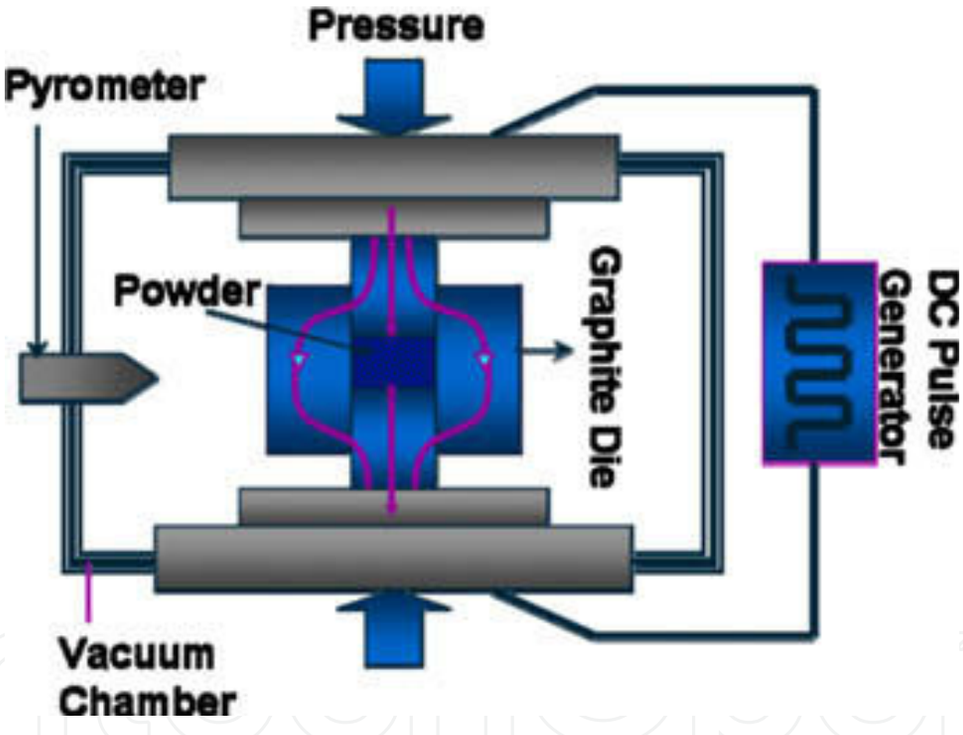

Figure 9. Schematic of the PCAS process

As an advanced technology for materials synthesis and processing, RS presents a lot of potential applications. But its sintering mechanism is still in dispute. It is generally acknowledged that in the sintering procedure, when an electric current runs through, the consequent Joule heat effect and the plastic deformation caused from temperature-rising and loading help the sintering process, but other elements play a much greater role. For example, when pulse DC voltage is on, spark discharge/plasma generates between adjacent particles [19,20], and individual ones are spontaneously heated, leading to the activation, purification of particle exterior surface and removing of oxide film, helping the rapid material diffusion and

migration, promoting efficient heating and plastic deformation. When the pulse voltage is off, the temperature decreases rapidly through thermal diffusion and sintered material is subjected to quite short temperature exposure [21]. All of the phenomena and effects realize the consolidation of specific products with desired configuration and density at lower temperature and in shorter sintering time, as introduced in details in Fig. 10.

It is accepted that pulsed current concentrates on the junction of neighboring powder particles. Activated by pulsed electric current field, anode and cathode emerge in minute zones, where spark discharge and plasma are generated. The energetic particles from discharging knock on the contact part between adjacent particles, then the resulting local high temperature bring the superficial layer into a molten state, causing the emergency of 'neck' [22], as illustrated in Figs. 11. The transmission of the thermal energy from the particle center to the surface and its rapid dissipation result in a quick cooling in the 'neck's, prompting consolidation and material migration and transfer between neighboring powder particles through volume diffusion, surface diffusion and grain boundary diffusion [20], as Fig.12 shows. It is the simultaneous effect of electric current heating and uniaxial loading from the upper punch that reinforces volume diffusion and boundary condition so that the sintering synthesis and densification is accelerated and the sintered compacts of high quality can be gained in shorter duration of time and at lower sintering temperature.

However, how to verify the existence of discharged plasma has been a problem all the time. Besides, it has been proved on the basis of experimental studies that electric current cannot run through non-conductive powders, thus the view of generation of plasma in such powders does not work. Therefore, many scholars doubt the above-mentioned theory. For this reason, a 'self-adjusting' mechanism in microstructure evolution comes forward [23], as shown in Fig. 13. It is recognized that in the initial stage of sintering, many particles have come into contact under pressure. The electric current tends to be relatively larger in the particle who has contributed larger contact surface, that is $I_1 > I_2$. Thus, the sintered 'neck' forms firstly in the particle which I_1 passes through for the reason of the Joule heat effect. With the neck growing up, the contact surface increases further, then current I_1 ascends and neck temperature augments correspondingly, producing increased local resistivity and resistance. At the moment, current in I_1 particle is frustrated and commences to run through the particle with smaller contact surface, namely, $I_2 > I_1$. As a result, neck forms in the particle with smaller contact surface. And so on alternately until powder consolidation and densification process is completed. Such a mechanism can explain the cause why the sintered materials are always with fine, homogeneous and dense microstructures. But the explanation can apply only to conductive material with positive resistance-temperature coefficient. When it comes to non-conductive materials with no obvious resistance changing sensitivity to temperature, it does not work. It is generally believed that the rapid transportation of heat through mold and upper and lower punches, together with the large electric current, bring non-conductive powders directly into the high-temperature zone and make it possible to realize rapid synthesis.

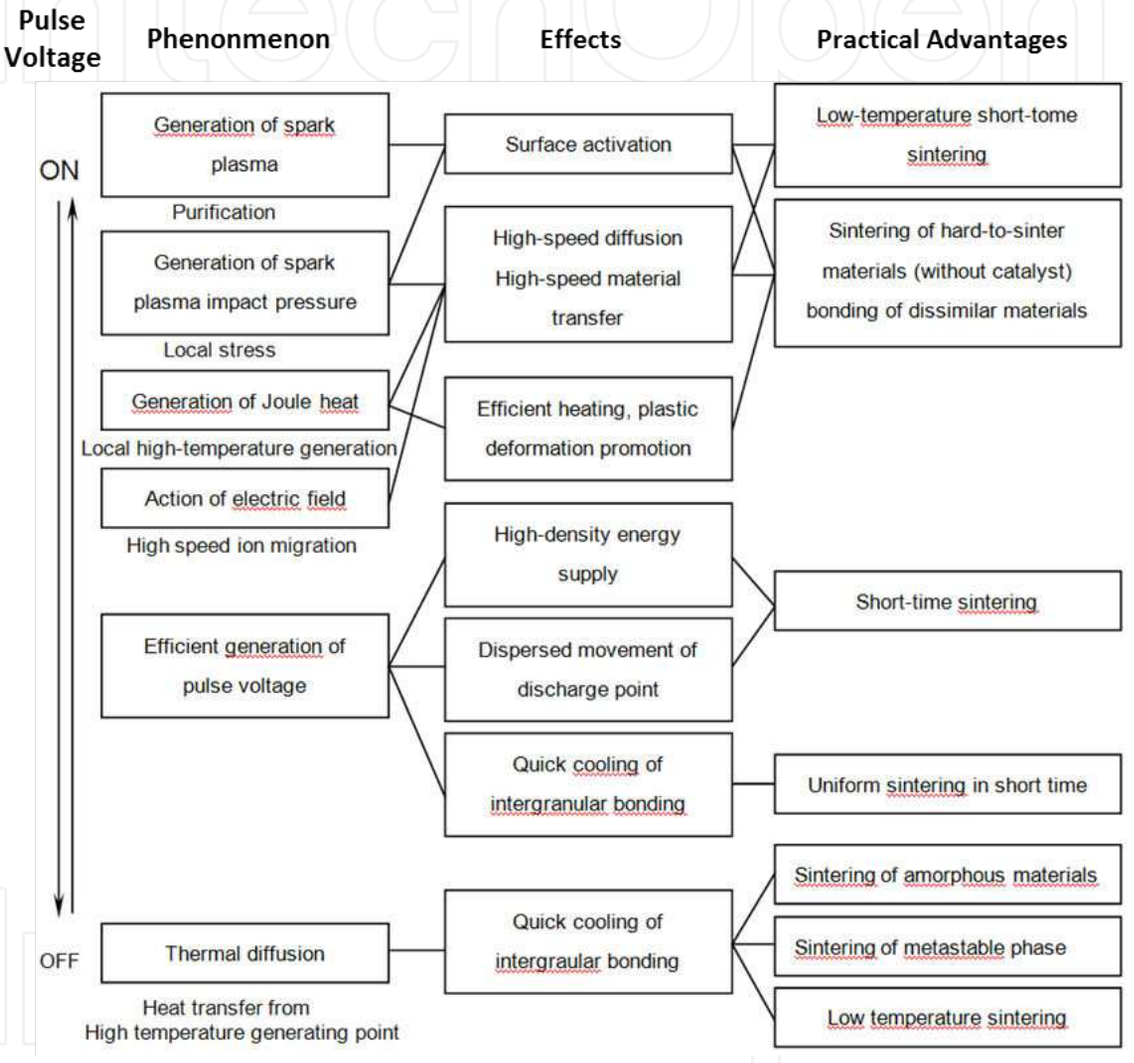

Figure 10. Effect of ON/OFF direct current pulse energizing

http://dx.doi.org/10.5772/53469

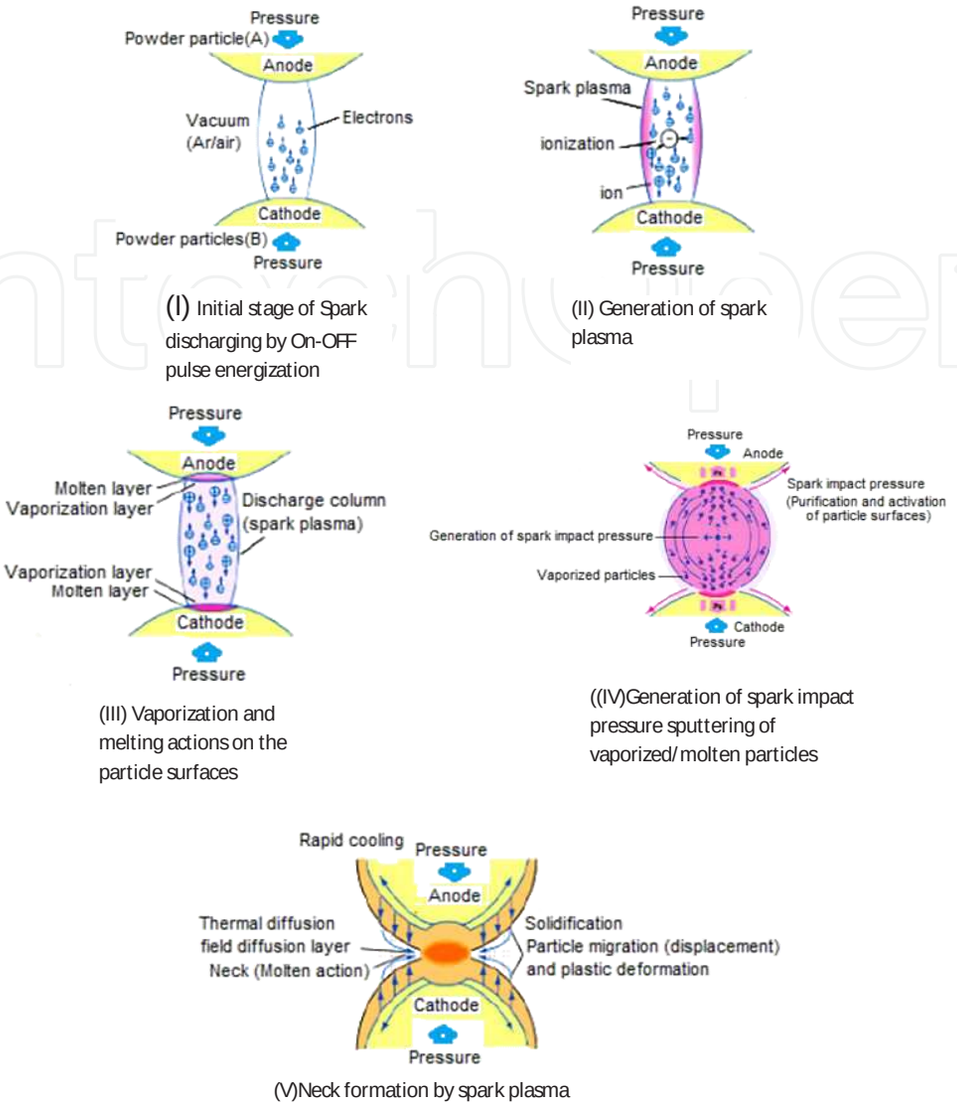

Figure 11. Mechanisms of neck formation between particles

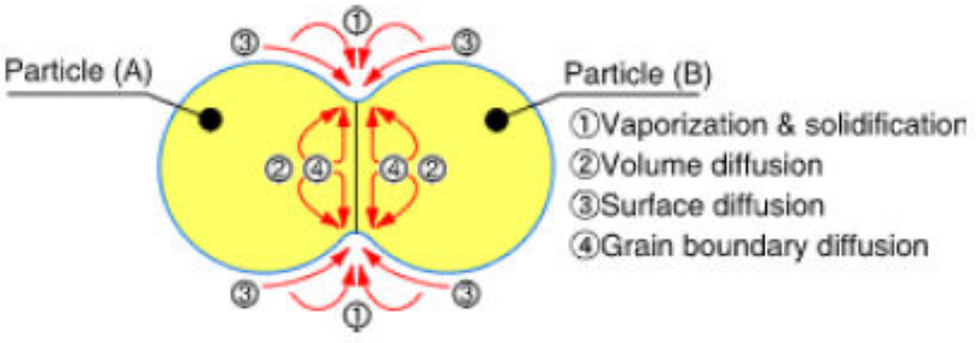

Figure 12. Material transfer paths during sintering process

Although the working mechanism of the technique is far from reaching a consensus, studies prove that electric pulse plays an importance effect on crystallization. Pulsed current possesses such a short relaxation time that it eliminates nucleation barrier and raises nucleation rate and refines sintered microstructures.

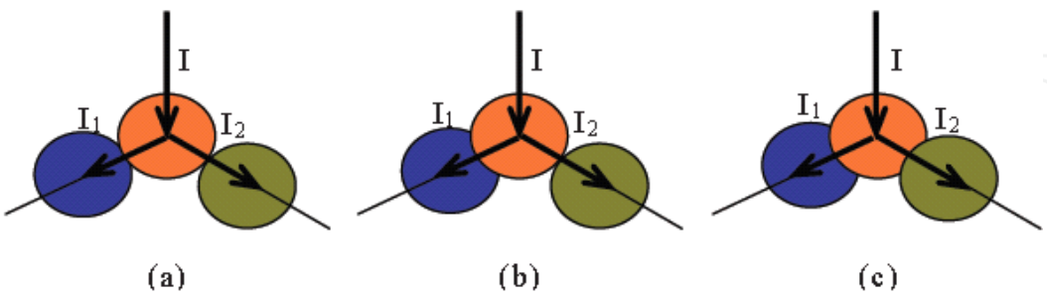

Figure 13. Change of contact areas between adjacent powders and distribution of electric current

1.4. characteristics and advantages over other sintering methods

This technology seems characterized by technological and economical advantages over conventional sintering methods, such as more efficient use of the heat input, faster heating rate, lower sintering temperature, shorter holding time, elimination of the need of sintering aids, no need of cold compaction, less sensitivity to initial powders characteristics, and marked comparative improvements in the properties of consolidated materials [24]. Especially when electrically insulating container is used and the electric current is applied for extremely short duration (down to few hundreds of microseconds), these advantages are more obvious.

For costly materials, this means considerable cost savings from reduced machining requirements and materials scrap. In addition, it should be noted that for engineering purposes shorter processing times usually result in productivity gains. As a consequence, sintered parts of higher quality may be expected to be obtained at lower processing costs.

On the contrary, in conventional powder metallurgy techniques, the powder container is typically heated by radiation from the enclosing furnace through external heating source. The resulting heating rate is then typically slow and the process can last hours. In the process, a lot of heat is wasted as the whole volume of space is heated and the compact receives heat indirectly from the hot environment.

2. Application to synthesis of γ-TiAl alloys

γ-TiAl alloys are of great interest for applications in aerospace industry due to their numerous advantages, such as low density, high specific Young's modulus and strength, good oxidation and burn resistance. However, such intermetallics suffer from having only poor machinability at room temperature and limited ductility at high temperatures, which limits their practical application [25]. In order to solve the problem, improving their room-temperature ductility and developing their superplasticity at high temperatures is of much importance.

http://dx.doi.org/10.5772/53469

Investigations have shown that fine grain size is beneficial for alloys to display good tensile behavior for the facility of grain sliding and diffusion [26]. However, it is difficult to directly obtain micron or submicron grains in γ-TiAl alloys through traditional cast or powder metallurgy route without subsequent heat treatment or complicated and costly mechanical processing. Thus, simplifying preparation route becomes an urgent need.

Up to now, electric current auxiliary sintering technique (ECAS) has been applied to synthesize γ-TiAl alloys and specimens with high densities and microstructures approaching the equilibrium state have been obtained [27-31]. The influence of operating parameters (i.e. temperature, processing time, etc.) on sintered γ-TiAl characteristics has been studied. However, heating rate effect was not widely explored. The typical heating rate is as low as1.7℃/s [27] or even less [32]. As a result, γ-TiAl alloys with coarse lamellar colonies were often obtained, even though the starting powders were managed to be refined. Thus, subsequent mechanical processing or other treatments become necessary for the purpose of improving the product properties. Currently, processed γ-TiAl alloys produced by electric current auxiliary sintering or other conventional processing routes, usually exhibit poor ambient ductility (in the range of 0.3~2% elongation).

In this context, dense γ-TiAl alloys with diverse microstructures through the controlling of sintering temperature, dwell time and heating rate are synthesized in PCAS apparatus from initially coarse powders (with particle size in the range of 5-350μm and the mean size of 103μm). When great care is taken, marked improvements in the tensile properties can be obtained both at room temperatures and at high temperatures. Above-mentioned experimental details are investigated and relevant results are given. Besides, an attempt was made to explain the effect of experimental parameters control, especially the role of heating rate, using thermodynamic theories, as well as nucleation and growth kinetics.

2.1. Experimental details

Pre-alloyed powders (Fig. 14) with the composition of Ti-42.5Al-2.3Nb-2.2Cr-0.28W- 0.15B (in at.%, mean grain size = 103μm, oxygen concentration ≈ 700ppm (wt.%)) were filled into a graphite mold sealed by two graphite punches at both ends. The loose powders in the graphite mold with a rectangular cross-section in the dimension of 10mm×30mm were subjected to pulsed direct current with different current densities to realize three groups of contrast experiments. The tested heating rate ranged from 2 to 9℃•s^{-1}; sintering optimal temperatures have been tested at 1200, 1250 and 1300℃; heating dwell time have been tried for 5min, 10min and 15min. In the experiments a gradual increasing pressure at the onset of the pulse was exerted until the optimal temperature and a specified pressure of 50MPa were attained nearly simultaneously. Then, the temperature and pressure were held constant for certain duration, followed by furnace cooling. A pulsed direct current with on/off cycles of 1.5ms (on-time) / 0.5ms (off-time) was applied. All the details for the three groups of contrast tests have been listed in Table 2.

Tensile specimens with a gauge length of 8mm and a section area of 3×1.2mm^2 were machined from the compacts. Tensile tests were carried out in air on American Instron 5500R testing machine at a strain rate of $2.083\times10^{-4}s^{-1}$ at ambient temperatures and high tempera-

tures from 800 to 1000℃. SEM observations were operated on S4700 scanning electron microscopy (SEM), equipped with backscattered electron image. Conventional TEM (transmission electron microscope) observations were made on a Philips CM 12 operating at 120kv. Thin foils for TEM observation were cut parallel to the tensile axis from the gauge section. The foils were prepared by the standard jet polishing method using a solution of 30 vol.% nitric acid, 70vol.% methanol under ~15V and at -30℃.

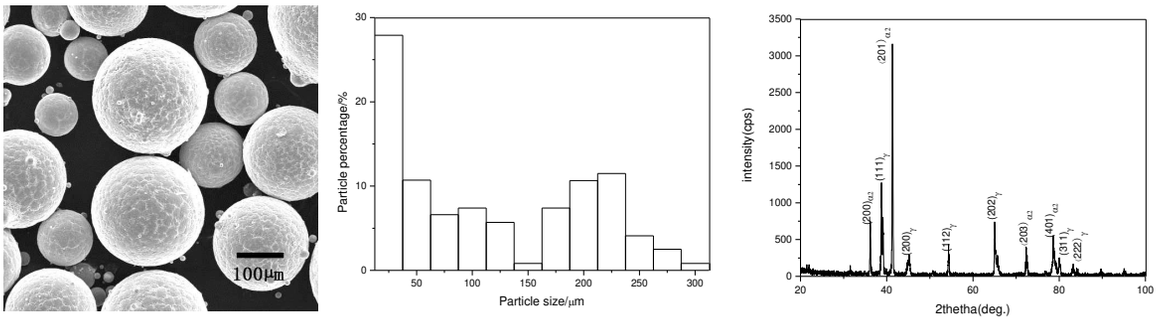

(a) (b) (c)

Figure 14. Basic information about pre-alloyed powders: (a) SEM micrographs, (b) particle size distribution (c) powders XRD analysis

Group	Heating rate (°C · s^{-1})	Sintering temperature (°C)	Dwell time (min)	Loading pressure (MPa)
1	9	1250	5	50
	4.5	1250	5	50
	3	1250	5	50
	2.5	1250	5	50
	2	1250	5	50
2	3	1200	10	50
	3	1250	10	50
	3	1300	10	50
3	3	1250	15	50

Table 2. Technological parameters adopted in sintering processes

2.2. Results and discussion

2.2.1. Dependence of as-sintered microstructures on sintering parameters

2.2.1.1. Heating rate

Typical back-scattered photomicrographs of four representative specimens sintered with heating rates of 2-9℃•s^{-1} are given in Fig. 15. It can be clearly observed that heating rate has a significant influence on the sintered microstructures. In the specimen sintered with heating-up rate of 9℃•s^{-1}, boundaries of original alloy powders can be clearly observed and a

http://dx.doi.org/10.5772/53469

volume of pores between adjacent particles still exist. The compact is far from being consolidated. It can be remarked that inside individual powders, recovery and recrystallization have occurred, but grains have mal-developed. When powders were sintered with lower heating rate, 4.5℃•s^{-1}, grains developed fully and fine grains formed. When a local region is zoomed in, Fig. 16 can be obtained, presenting a dense micron-sized near-γ microstructure with irregular grayish-white α_2-Ti_3Al interspersed in the matrix of nearly equiaxial gray γ-TiAl. The $[01\bar{1}2]_{\alpha_2}$ and $[00\bar{2}]_{\gamma}$ zone diffraction patterns of the two phases are shown in Figs. 16 (c) and (d), respectively. A linear intercept method was used to reveal grain size d=4μm for γ and a volume fraction V_{γ}= 88.7%.

3℃•s^{-1} sintered materials were alloys with a duplex microstructure with nearly equi-axed gray γ grains dotted about α_2/γ lamellar colonies. TEM diffraction patterns of the two phases in lamellar region in Fig 15 (c) are shown by Fig.17, in which $[000\bar{2}]_{\alpha_2}//[\bar{2}\bar{2}\bar{2}]_{\gamma}$ is labeled, demonstrating $(111)_{\gamma}//(0002)\alpha_2$ and $[10\bar{1}]_{\gamma}//[11\bar{2}0]_{\alpha_2}$. The microstructure of specimens heated within 2-2.5℃•s^{-1} consists of fully regular patterns of α_2/γ laminates and no equiaxed γ grains. The slower the heating rate, the coarser the lamellar colony size is. Lamellar colony and grain sizes in samples consolidated with the heating rate of 2-4.5℃•s^{-1} are listed in Table 3. All the last four specimens have relative densities over 98% of the theoretical values, and microstructures are all uniform.

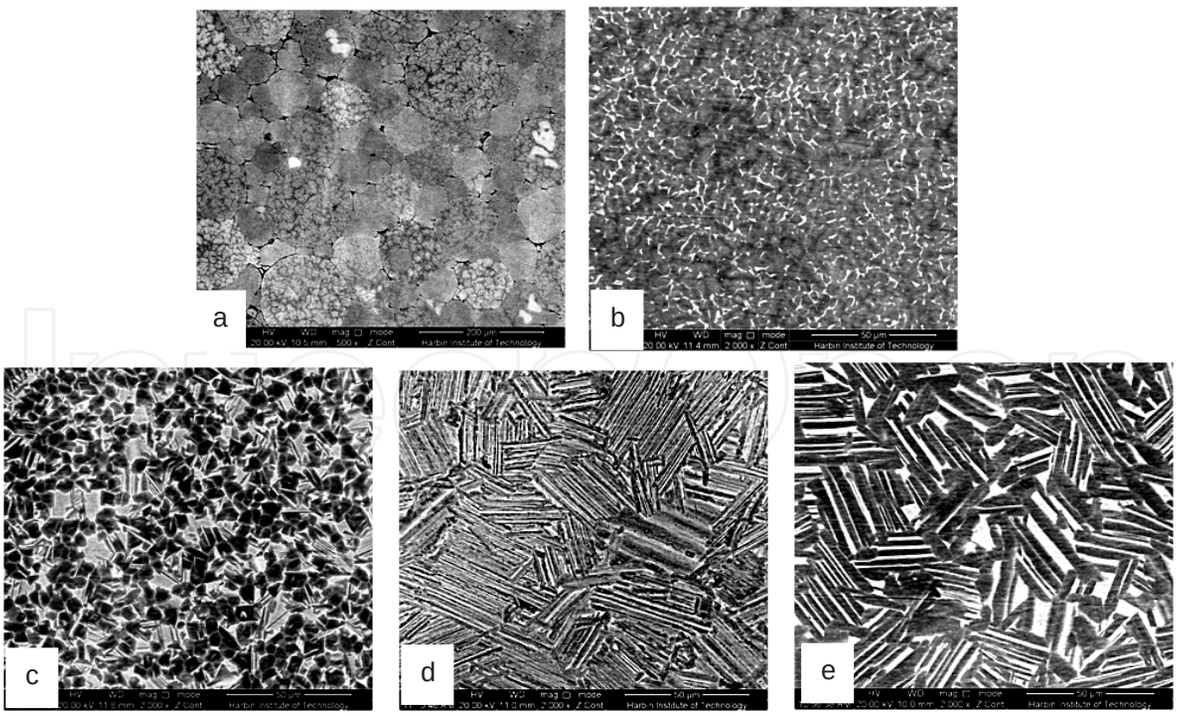

Figure 15. Back scattered SEM images of microstructures in alloys sintered at 1250°C for 5min with the heating-up rate of (a)9°C · s^{-1}, (b)4.5°C · s^{-1}, (c) 3°C · s^{-1}, (d)2.5°C · s^{-1}, (e)2°C · s^{-1}

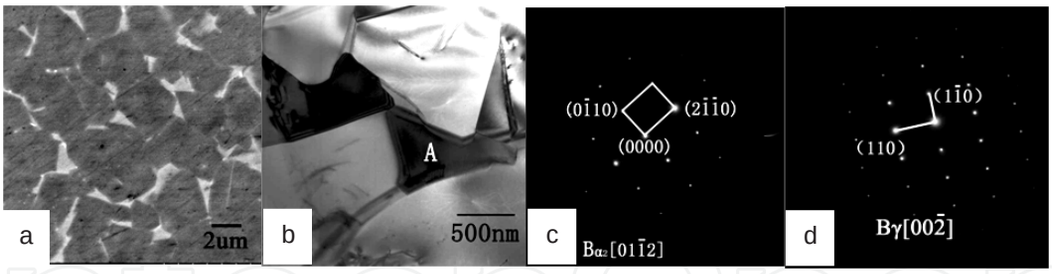

Figure 16. Microstructures in alloy sintered with heating rate of 4.5°C · s^{-1}: (a) Zoomed back scattering SEM image, (b) bright-field TEM image, (c) diffraction patterns of α_2 (grain A in (b)), (d) diffraction patterns of γ

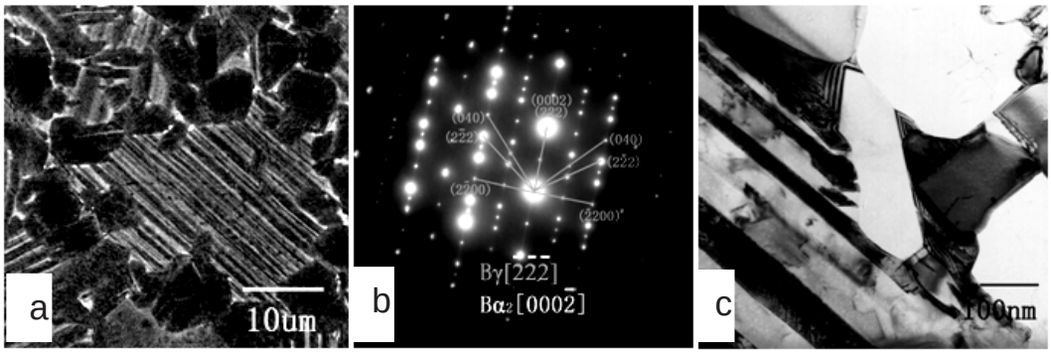

Figure 17. Microstructures in 3°C•s^{-1}-sintered alloy: (a) Zoomed back scattering SEM image; (b) bright-field TEM image; (c) diffraction patterns of α_2 and γ, in which $[000\bar{2}]_{\alpha_2}$ / / $[\bar{2}\bar{2}\bar{2}]_{\gamma}$

Heating rate (℃ · s^{-1})	Microstructure (μm)	Lamellar spacing (μm)	Lamellar Volume fraction (%)
4.5	NG(4)		0
3	DP(6~9)	0.21	22.3
2.5	FL(25)	0.89	100
2	FL (27)	2.53	100

Table 3. Controlled microstructures and corresponding values of the alloys sintered at 1250℃ for the duration time of 5min with different heating rates

2.2.1.2. Sintering temperature

When heating rate was fixed at 3°C · s^{-1}, duration time was lengthened to 10min, and loose powders were sintered at 1200°C, 1250°C and 1300°C, synthesized material display different microstructures, as shown in Fig. 18. In the compact sintered at 1200°C, original powder boundaries can still be seen although shapes of powders have changed from spheres to polyhedrons under pressure. Material migration was not finished fully enough to form grains and granular boundaries. When the sintering temperature was raised up to 1250°C, a uniform and full lamellar microstructure formed. The mean lamellar colony size is 30μm. When the material is sin-

http://dx.doi.org/10.5772/53469

tered at 1300°C, a full lamellar microstructure with average colony size of 50μm was consolidated with obvious coarser lamellar spacing than the product obtained at 1250°C.

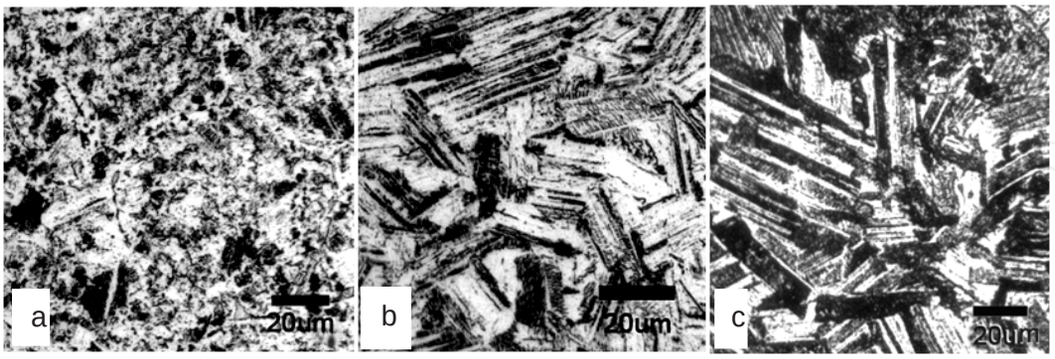

Figure 18. Microstructures of alloys heated with the rate of $3°C \cdot s^{-1}$ and sintered at different temperatures for 10min :(a)1200°C, (b)1250°C, (c)1300°C

2.2.1.3. Dwell duration

The Fig. 19, combined with micrographs in Fig. 15(c) and Fig.18(b), the influence of duration time on the sintered microstructures can be deduced. In the sintered compact heated at the rate of $3°C \cdot s^{-1}$ up to 1250°C and stayed at the temperature for 5min, the microstructure presented a duplex feature, composed of fine lamellar colonies and equiaxed γ grains. When the duration period is extended to 10min, a complete lamellar microstructure was generated. If the dwell time was further lengthened, a complete lamellar with coarser colony size was observed. The average lamellar colony size got to 120μm, the spacing augments to 2.2μm.

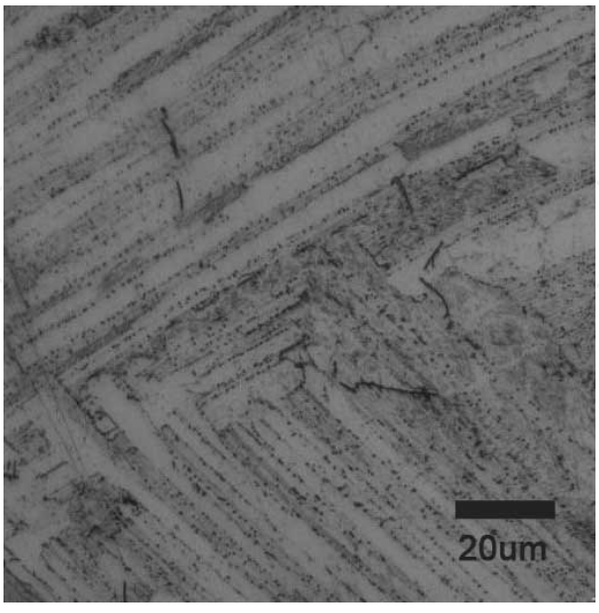

Figure 19. Microstructures of alloys heated with the rate of $3℃ \cdot s^{-1}$ and sintered at 1250℃ for 15min

2.2.1.4. Discussion

Working mechanisms for the PCAS technique has been introduced in details in the first part of the chapter. But when the effect of sintering parameters on consequent microstructures is involved, the above-mentioned theory seems a little abstract to explain the corresponding evolution of microstructures. Hereinafter, the author tried to approach the effect of sintering parameters on resultant microstructures from the viewpoint of thermodynamics, as well as nucleation and growth kinetics.

Firstly, attention was paid to the effect of heating-up rate. If the joule heat generated by the pulsed electric current flowing through the tested material is denoted by Q_t, $Q_t=Q_r+Q_h$, where Q_r is the heat input during transient (i.e. temperature-rise) period, and Q_h is that supplied during steady-state sintering. Since four sintering processes about heating rate influence were all carried out at 1250℃ for 5min under the load of 50MPa, $Q_h$was the same. The only consideration is thus Q_r.

According to classical equation: $Q = I^2Rt$. I is the applied electrical current and $I = \varrho_I * S$, where ϱ_I is the current density, which has been listed in table 4, and the cross-sectional area in tests $S = 30\times10mm^2$. The material's electrical resistance R can be derived in terms of the equation: $R = R_0(1+aT)$, where T is the thermodynamic temperature, R_0 the material resistance measured at 0℃, and 'a' is the temperature resistance coefficient. For the shortage of a suitable strong testing machine, it is sensible to choose R_0 as a constant. For simplicity, the averaging value of the coefficient 'a' was taken according to the equation: $a= (R_2-R_1)/R_1\Delta T$. $\Delta T =T_2 - T_1$, herein $T_1 = 293k$, $T_2 = 1523k$ in experiments. In addition, R_1, R_2 respectively refer to the electrical resistance of initial loose powders and that of the alloy products. If all the alloy products are presumed to get to theoretical densification, it can be sure that R_2 must also be the same. Thus 'a' is identified as another constant term. The numeral value of the time 't' spent in temperature-rise period has been listed in table 4 as well. So the heat yielded by the current in temperature-rise period is calculated as follows:

$$Q_r = I^2Rt = \int_{T_1}^{T_2}\int_0^t I^2R_0(1+aT)tdtdT = \int_{T_1}^{T_2} I^2R_0(1+aT) = \frac{1}{2}t^2I^2R_0[(T_2-T_1)+\frac{1}{2}a(T_2^2-T_1^2)]$$

If the equation is reduced to $Q_r= (A+Ba)R_0$, table 5 will be obtained. Based on theory of electron and quantum, literature [33] confirms that resistance temperature coefficient for metals is about 0.4%. Then, 'a' in the above-equation must be a positive constant. Therefore, the result is straightforward that slower heating supplies a higher energy.

Usually the heat energy is consumed by three respects: Q_S, Q_T and Q_L, where Q_S is the energy for synthesis and densification of powders, Q_T is for morphologic transformation, and Q_L is for thermal losses. Here, Q_L can be neglected because the graphite mold used in the experiments was set inside a ceramic mold to prevent heat losses. Allowing for all the powders have been synthesized to compact alloys under the four sintered conditions, Q_S must be the same. Therefore, the more heat energy absorbed in $2℃\bullet s^{-1}$, $2.5℃\bullet s^{-1}$, $3℃\bullet s^{-1}$-sintering process than that in $4.5℃\bullet s^{-1}$-sintering period is used for morphological transformation. The slower the heating up rate, the more energy for such transformation will be.

Heating rate(°C·s^{-1})	ρ_I (A·mm^{-2})	t(h)
2	7.3	0.174
2.5	7.7	0.139
3	8.1	0.116
4.5	9.1	0.077

Table 4. Correlative numeral values in temperature-rise period

Heating rate(°C·s^{-1})	A(×10^6)	B(×10^9)
2	0.835	1.271
2.5	0.742	1.130
3	0.685	1.043
4.5	0.574	0.874

Table 5. Numeral values of A and B in Q_r

In the experiments in the current chapter, the more energy corresponds to more lamellar volume fraction in sintered alloys. Also it has been mentioned above that our starting metal powders consists of γ and α_2 (Fig.14(c)) with the approximate composition of Ti-42.5Al. In terms of Ti-Al binary phase diagram, Fig. 20, when experimented materials were heated up to 1250℃, the sintering temperature, the constituent phases γ and α_2 would both turn into disordered phase α. Thus it can be asserted that phase transformation in the sintering process followed the route: $\alpha \rightarrow \alpha+\gamma_{PPT} \rightarrow \alpha+\gamma_P \rightarrow$ Lamellar (α/γ) $\rightarrow$ Lamellar($\alpha_2+\gamma$), where γ_{PPT} refers to disordered γ (equiaxed grains), $\gamma_P$ordered γ (γ plates).

When after heat preservation and the material was cooled down into $\gamma+\alpha$ two phase region, in α, the whole dislocation a/3<1120 > was discomposed into partial Shockley ones with simple stacking faults (SF): $\alpha \rightarrow \alpha^{SF}+\alpha \rightarrow \gamma_{ppt}+\alpha$ [34]. Such SFs would change local stacking sequences in $(0001)_\alpha$ in hcp α matrix, leading to a local change of crystal structure from hcp$\rightarrow$LI$_0$. γ grains began to precipitate. Driven by surface tension, the precipitated disordered γ phase turned equiaxed. If at such time not enough energy can promote more equiaxed γ grains to precipitate further, such γ grains together with residual α would change into γ and ordered α_2, making up near γ microstructure. But the formation of equiaxed γ brought about differences in chemical free energy between γ and α matrix, and further redistribution of Ti and Al atoms. Thus it can be figured out that equiaxed γ is only a pioneer of lamellar γ/α_2 colonies. If the energy absorbed by the material can keep it in $\gamma+\alpha$ region for longer time, the internal structure tends to change into a more stable state.

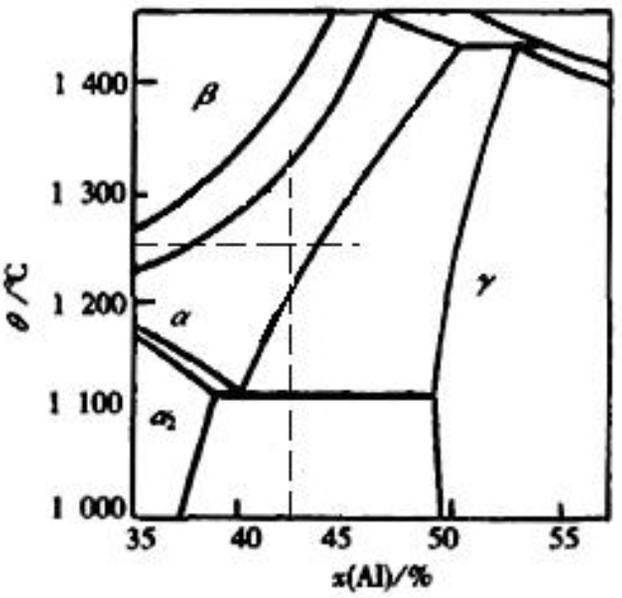

Figure 20. Central part of Ti-Al binary phase diagram

The surface of equiaxed γ grains is composed of many crystal faces with varied orientation, and such places can easily become nucleation location for γ lamellae. Extension of partial Shockley dislocations led to γ lateral growth and formation of "terrace" in phase boundaries. The formed kinking parts attracted atoms' diffusion and migration, resulting in γ growing laterally and γ plates formed. That is, γ plates form and grow by the "terrace-ledge-kink" mechanism [35]. In view of the fact that γ lamellae grew into neighboring α matrix interior with different rates and the growth rate in coherent α was greater than in incoherent ones, the differences in chemistry free energy would drive α on the side with incoherent boundaries to grow into γ interior. Then lamellar γ/α_2 colonies took shape[36,37]. γ plates can parallel align along $(0001)_{\alpha}$, the only habit plane in hcp α, while α lamellae can align along four habit planes in γ, including $(111)_{\gamma}$, $(\bar{1}11)_{\gamma}$, $(1\bar{1}1)_{\gamma}$ and $(11\bar{1})_{\gamma}$.As a result, the alignment of the two phases formed Blackburn phase relation [38, 39]. If excess energy existed at this time, all of equiaxed γ would be consumed and the whole microstructure in sintered alloys would be composed of lamellar γ/α_2 colonies. And there could be no doubt that more excess energy can thicken lamellae further. Then when the structures were cooled down to the room temperature, γ would remain and α would evolve into ordered α_2. Correspondingly, duplex or fine lamellar or coarse lamellar microstructure would be observed. Certainly, what microstructures can be obtained depends on how much energy the sintered material has absorbed.

The above-mentioned phase transformation process is in agreement with experimental results in this paper. Fig. 21 displayed such microstructure evolution process in TiAl alloys [40]. It should be pointed out that in the PCAS technique, electric field helps to improve nucleation rate and refine microstructures. As a result, the recrystallized α would be finer than that given in the figure, then more equiaxed γ would be separated out. When fine γ grains reached out to each other, triple junctions among boundaries would appear and near gam-

ma would form. Therefore, the reason for the as-sintered microstructures changing from near gamma to duplex, fine lamellae, then coarse lamellae with the increment of heating-up rate can be clearly uncovered. The effect of lengthening duration time and raising sintering temperature is the case also.

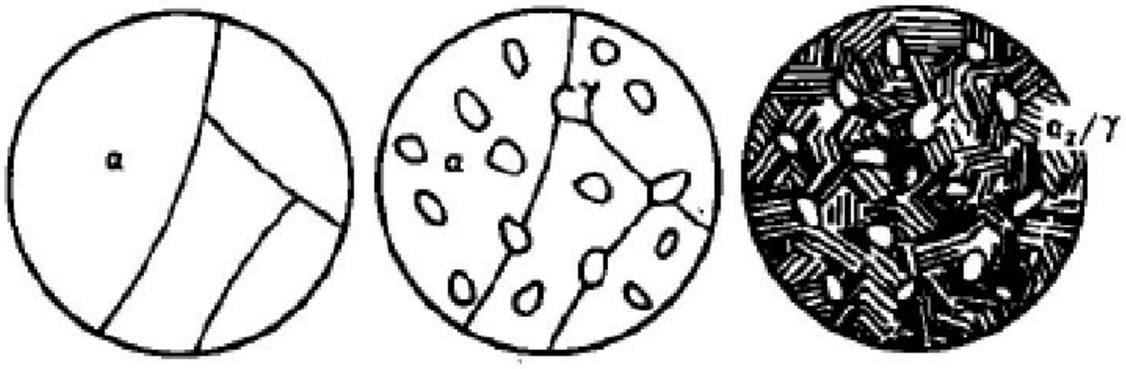

Figure 21. Schematic drawing of microstructure evolution process in TiAl alloys

2.3. Tensile properties of as-sintered alloys

Due to the fact that the alloys sintered at 1250 °C with heating rate of 2-4.5℃ · s^{-1} and dwell time of 5 min present relative fine-grained microstructure. So, all these samples were subjected to room temperature tensile tests. 4.5°C · s^{-1}- and 3°C · s^{-1}- sintered samples were picked out to experience high temperature tensile tests. It was found that some alloys displayed improved tensile properties than results from other researchers.

2.3.1. Room temperature tensile properties

Tensile properties of the sintered alloys are listed in Table 6. As shown in the table, room-temperature mechanical properties of the materials are dependent upon the microstructure. Ultimate tensile strengths σ_b of all specimens fell between 300 and 700MPa. The ultimate tensile strength increases with a decrease in lamellar colony size. Whereas the two samples with lamellar structure exhibited ordinary tensile elongation, the ductility of samples with near γ and duplex structures were over the usual value of 0.3-2%.

Heating rate(°C · s^{-1})	Microstructure (μm)	σ_b(MPa)	δ(%)
4.5	NG(4)	578	3.59
3	DP(6~9)	632	4.51
2.5	FL(25)	416	2.21
2	FL(27)	367	1.58

Table 6. Results of ambient temperature tensile tests at 2.083×10^{-4} s^{-1}

It has been shown [41] that the refinement of grain size can enhance the mechanical properties of TiAl. Indeed tensile properties of the two coarse fully lamellar microstructures are lower than those of duplex microstructure (Table 6). The strengthening mechanism of TiAl alloys with refined microstructures may be attributed to the classical Hall-Petch equation $\sigma = \sigma_o + KD^{-1/2}$, where σ_o refers to a material intrinsic value, K a Hall-Petch constant, and D the average diameter of grains. Such equation can be used to explain higher ultimate tensile strength when α_2 / γ lamellae size decreases from 27 down to 9μm. In addition, fine microstructures are beneficial for the operation of grain boundary sliding and the compatibility of deformation, resulting in better strain [42-44]. Furthermore, allowing for lamellar microstructures possessing the anisotropic mechanical property, differently oriented lamellae in deformation will produce discontinuous strain [45], resulting in the generation of interfacial microcracks and brittle failure of the tested specimen. Thus, better room temperature ductility is suppressed.

However, the above-mentioned theory isn't applicable for all the experimental results here in that in the test a room temperature ductility peak was observed in the duplex TiAl alloy instead of finer equi-axed one. Specifically, the maximum tensile strength occurs also at the maximum tensile elongation. In order to explain such phenomenon, close attention is paid to sintering processes. During sintering, load and heat were applied simultaneously. Therefore, high heating rate corresponded to high pressurizing rate. A high heating rate is expected to inhibit grain growth. As a result, grain sizes are much refined when heating rate is high. However, high loading rate can quickly seal the venting channels among powder particles and prevent a complete outgassing. This, of course, was not in favor for specimen densification during sintering [46]. Thus, the relative density of specimens obtained at the heating rate in the range of 2-3℃•s^{-1} was over 99.5%, while the density of that one sintered at 4.5℃•s^{-1} was 98.6%. The lower density, thus more residual pores reduces the ductility and tensile properties. Also, near gamma microstructure is a product of unstable phase transformation, so vast defects would remain in internal structures, such as a large number of dislocations tangled up in grains, as shown in Fig. 22. So, even though grain boundary sliding and deformation compatibility ameliorated with grains being refined, numerous dislocations tangling up inhibited the alloy's capability of homogeneous deformation [45]. As a result, the tensile properties of fine-grained, near γ sample are inferior to those with a duplex structure.

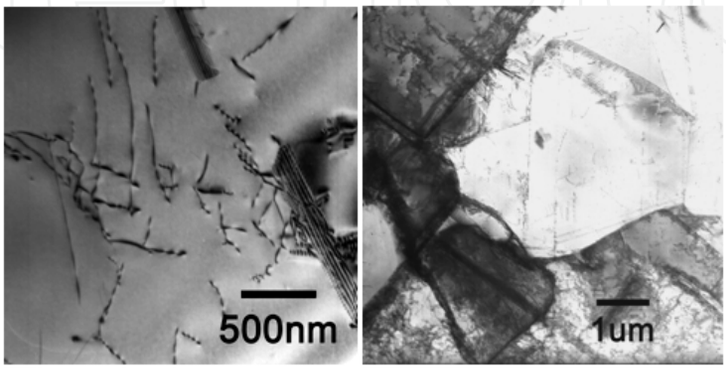

Figure 22. TEM micrographs of 4.5℃•s^{-1}-sintered alloy

2.3.2. High temperature tensile properties

Fig. 23(a) shows the true stress-strain curves of the 4.5℃•s^{-1}-sintered alloy for tensile deformation at temperatures ranging from 800 to 1000℃ at the strain rate of $2.083\times10^{-4}s^{-1}$. It can be seen that in the temperature range, plastic strain appeared, following the elastic deformation. Moreover, at above 900℃, steady flow took place. Besides, the equiaxial γ-TiAl based alloy under study is characterized by a remarkable elongation-to-fracture and a marked strain rate sensitivity m. As the temperature rises, the elongation exhibits monotonous character, increasing from 71% at 800℃, 165% 900℃, 241% 950℃ to the maximum elongation-to-failure δ=409% at 1000℃. The profile of the specimen fracture at 1000℃ is illustrated by the Fig. 23(b).

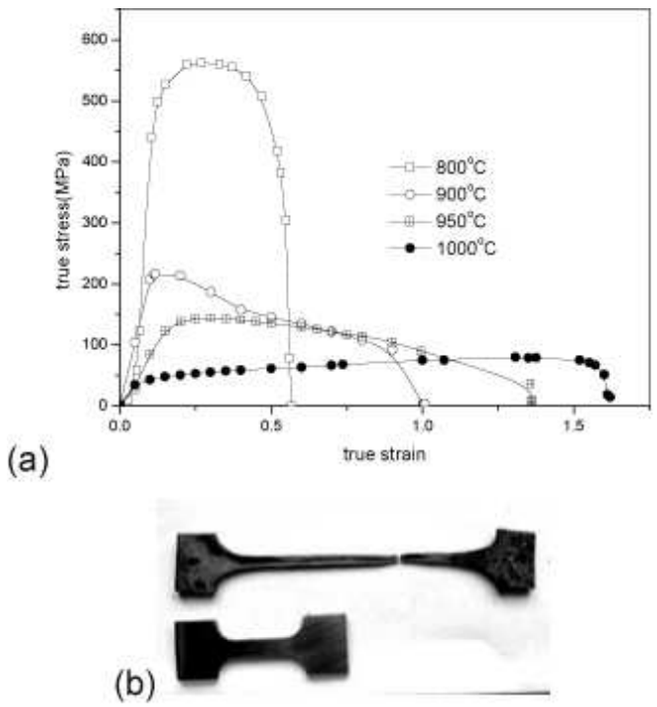

Figure 23. (a)True stress-strain curves of the 4.5℃•s^{-1}-sintered alloy for deformation at 800 -1000℃, (b) fracture sample deformed at 1000°C with 409% elongation and an as-prepared test piece (bottom) is also shown for comparison.

m value obeys the same tendency as the elongation, from 0.15, 0.33, and 0.45 up to 0.8 at 1000℃. The values of m and elongation-to-failure at temperatures above 900℃ are indicative of superplastic deformation behavior. Meanwhile, an increase of temperature leads to a rapid decrease in flow stress, decreasing from 565Mpa at 800℃ down to 79Mpa at 1000℃. This result is in accordance with the majority of γ-TiAl based alloys with micron-grained structure investigated to date [47-49].

The effect of testing temperature on the high temperature flow behavior of duplex microstructure is illustrated in Fig. 24(a). It can be seen that this alloy failed during the elastic stage at 750°C and the elongation reaches 10%.At 900°C, plastic strain began to appear, following the elastic deformation. At and above 950°C, steady flow took place. Moreover, an

increase in the temperature led to an increase in the elongation, from 48% at 900°C to 99% at 950°C, with a maximum of 135% achieved at 1000°C (Fig. 24 (b)). m value reached 0.23 at 1000°C, lower than the critical value 0.3 for conventional superplastic deformation. Its flow stress followed the same tendency as 4.5°C•s^{-1}-sintered alloy, namely decreasing with the test temperature ascending. However, compared with the tensile behavior exhibited by 4.5°C•s^{-1}-sintered alloy, flow stress in 3°C•s^{-1}-sintered one is always higher at corresponding test temperature.

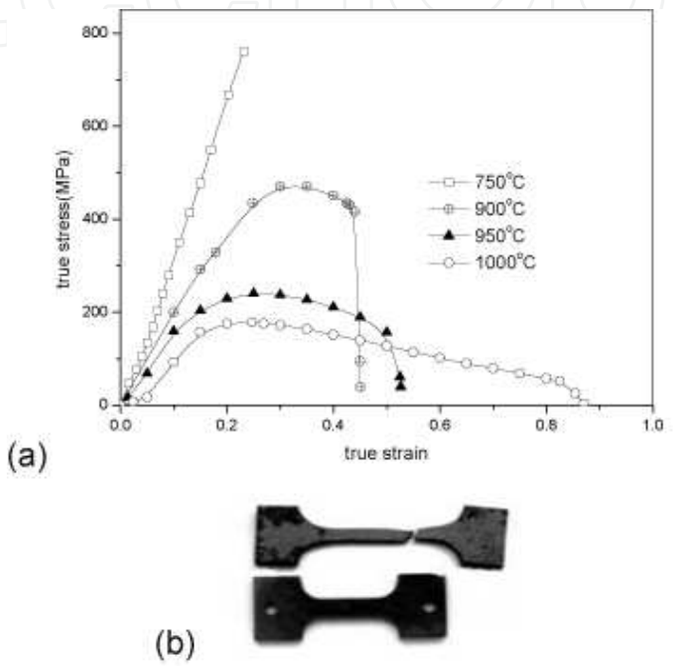

Figure 24. (a) True stress-strain curves of the 3°C•s^{-1}-sintered alloy for deformation at 750 -1000°C at the strain rate of 2.083×10^{-4}s^{-1} (b) fracture sample deformed at 1000°C with 135% elongation and an as-prepared test piece (bottom) is also shown for comparison.

Superplastic behavior was found in nearly equi-axed TiAl alloy with the usual prerequisites of fine grain size [50]. It is obvious that a decrease in grain size to a micron level improves deformation homogeneity, facilitates grain boundary sliding and interaction of dislocation with grain boundaries, decreases flow stress, and suppresses deformation twinning, providing increased ductility at relatively low temperatures [51]. Fine microstructures are beneficial to the compatibility of deformation. Large number of grains joins in the deformation, resulting in better plasticity.This is also the reason for the non existence of superplasticity in 3°C•s^{-1}-sintered duplex alloy.

Also, a microcrystalline grain size can help the alloy to display Superplastic behavior and decrease the temperature for Superplastic behavior with extensive grain boundary diffusion and sliding. Based on calculation of the activation energy Q for Superplastic deformation being 212.6~252.2kJ•mol^{-1}, the Superplastic deformation mechanism for the alloy is determined as the grain boundary sliding accommodated by grain boundary diffusion [52].

http://dx.doi.org/10.5772/53469

3. Conclusion

In the first part of this chapter, the technique of PCAS was firstly introduced in detail, including its origin, development, classification, fundamental working mechanism and a lot of advantages over other traditional material preparation technique.

The second part paid special attention to the application of the technique to synthesis of γ-TiAl alloys. On self-built pulse current auxiliary sintering apparatus (PCAS), influences of different parameters, including heating-up rate, sintering temperature and duration time, on obtained microstructures in sintered products were studied. After systematic researches on heating rates of 2~9°C · s^{-1}, sintering temperatures of 1200~1300℃, dwell times of 5~15min, it was determined that 1250℃ as the temperature and 5min as the duration time were more beneficial for generating dense, even and fine γ-TiAl based alloys.

When powders were synthesized in the oven at 1250℃ for 5min with heating rates of 4.5, 3, 2.5, 2℃ · s^{-1}, near gamma, duplex, fine fully lamellar and coarse fully lamellar microstructures were obtained, correspondingly. After comparison studies among these alloys, it was found that grain size, lamellar volume fraction and lamellar spacing played an important effect on room temperature mechanical properties of the sintered products. In general, duplex alloys possessed better comprehensive behaviors. Their ductility displayed at room temperatures could get to 4.51%. Thus, brittleness problem was solved to some extent.

In tensile tests at various temperatures on sintered TiAl alloys with near γ and duplex microstructures, it was observed that the one with equi-axed fine grains possessed more superior elevated temperature tensile properties. In temperature range of 950℃~1000℃ and strain rate range of $2.083\times10^{-4}s^{-1}$,the obtained elongation was over 240%. The results demonstrated its ability to display superplastic behavior at relatively low temperatures. Based on calculation of the activation energy Q for Superplastic deformation being 212.6~252.2kJ•mol^{-1}, the superplastic deformation mechanism for the alloy was determined as the grain boundary sliding accommodated by grain boundary diffusion

Based on the success in the synthesis of dense γ-TiAl alloys with fine microstructures, improved room-temperature and ideal high-temperature tensile properties, more studies are under way for processing industrial parts with good quality and improved mechanical properties directly by PCAS technique. These relative studies will explore more prospects for the application of the technique.

Author details

Zhang Chunping and Zhang Kaifeng

National Key Laboratory for Precision Heat Processing of Materials, Harbin Institute of Technology, Harbin, People's Republic of China

References

[1] Orru R., Licheri R., A. Locci M., Cincotti A., Cao G. Materials Science and Engineering R 63 (2009) 127–287

[2] L.Gao. Spark plasma sintering technique. Jounal of inorganic material. 1997;12:129-133

[3] Gao W., Gao X., Asif M., Wu Z.W., Ling B.L., Li J.G.. The Study of MARFE during Long Pulse Discharge in the HT-7 Tokamak. Journal of Nuclear Materials. 2007;363-365(15):770-774

[4] Clyens S., Al-Hassani S.T.S., Johnson W. The Compaction of Powder Metallurgy Bars Using High Voltage Electrical Discharges. International Journal of Mechanical Sciences. 1976;18(1):37-40

[5] Omori M., Okubo A., Kang G.H., Hirai T. Preparation and Properties of Polyimide/Cu Functionally Graded Material. Functionally Graded Materials 1996. 1997;767-772

[6] Tracy M.J., Groza J.R. Consolidation of Nanocrystalline Nb-Al Powders by Plasma Activated Sintering. Nanostructured Materials. 1993;2(5):441-449

[7] Kalyanaraman R., Yoo S., Krupashankara M.S., Sudarshan T.S., Dowding R.J. Synthesis and Consolidation of Iron Nanopowders. Nanosructured Materials. 1998;10(8): 1379-1392

[8] Kim H.C., Yoon J.K., Doh J.M., Ko I.Y., Shon I.J. Rapid Sintering Process and Mechanical Properties of Binderless Ultra Fine Tungsten Carbide. Materials Science and Engineering A. 2006;435-436(5):717-724

[9] Clyens S., Williams D.J., Johnson W. The Compaction of Some Powdered Foodstuffs. International Journal of Mechanical Sciences. 1976;18(9-10):449-450

[10] Kimura H. Powder Processing and Mechanical Characteristics of Fully Dense Nano-Intermetallics. Nanostructured Materials. 1997;9(1-8):93-96

[11] Jaraszewicz J., Michalski A. Preparation of a TiB_2 Composite with a Nichkel Matrix by Pulse Plasma Sintering with Combustion Synthesis. Journal of the European Ceramic Society. 2006;26(13):2427-2430

[12] Song Z., Kishimoto S., Shinya N. Fabrication of Closed Cellural Nichel Alloy Containing Polymer by Sintering Method. Journal of Alloys and Compounds. 2003;335(1-2):166-170

[13] Xie G.Q., Ohashi O., Chiba K., Yamaguchi N., Song M., Furuya K., Noda T. Frequency Effect on Pulse Electric Current Sintering Process of Pure Aluminum Powder. Materials Science and Engineering A. 2003;359(1-2):384-390

[14] Anselmi-Tamburini U., Gennari S., Garay J.E., Munir Z.A. Fundamental Investigations on the Spark Plasma Sintering/Synthesis Process:II. Modellling of Current and

Temperature Distributions. Materials Science and Engineering A. 2005;394(1-2): 139-148

[15] Chen W., Anselmi-Tamburini U., Garay J.E., Groza J.R., Munir Z.A.. Fundamental Investigations on the Spark Plasma Sintering/Synthesis Process:I. Effect of Dc Pulsing on Reactivity. Materials Science and Engineering A. 2005;394(1-2):132-138

[16] Vanmeensel K., Laptev A., Hennicke J., Vleugels J., Van der Biest O. Modelling of the Temperature Distribution during Field Assisted Sintering. Acta Materialia. 2005;53(16):4379-4388

[17] Gennari S., Anselmi-Tamburini U., Maglia F., Spinolo G., Munir Z.A.. A New Approach to the Modeling of SHS Reactions: Combustion Synthesis of Transition Metal Aluminides. Acta Materialia. 2006;54(9):2343-2351

[18] Michalski A., Jaroszewicz J., Rosinski M., Siemiaszko D. NiAl-Al_2O_3 Composites Produced by Pulse Plasma Sintering with the Participation of the SHS Reaction. Intermetallics. 2006;14(6):603-606.

[19] Tokita M. Development of Large-size Ceramic/Metal Bulk FGM Fabricated by Spark Plasma Sintering. Materials Science Forum. 1999;308-311:83-88

[20] Kim H., Kawahara M., Tokita M. Specimen Temperature and Sinterability of Ni Powder by Spark Plasma Sintering. J.Japan Socoety Power. Powder Metallurgy. 2000;47: 887-891

[21] Groza J.R., Zavaliangos A. Sintering Activation by External Electrical Field. Materials Science and Engineering A. 2000;287(2):171-177

[22] Song X., Liu X., Zhang J. Evolution of microstructure in conductive powders and its mechanism during SPS sintering. Chinese Science. 2005;35:459-469

[23] Li B., Wang X., Han X., Liu X., Li S. Synthesis of nano-grained $BaTiO_3$ by SPS technique. Piezoelectricity and acousto-optic. 2005;27:43-46

[24] Khor K.A., Cheng K.H., Yu L.G., Boey F. Thermal Conductivity and Dielectric Constant of Spark Plasma Sintering Aluminium Nitride. Materials Science and Engineering A. 2003;347:300-305

[25] Vassiliou M.S., Rhodes C.G., Mitchell M.R., Graves J. Metastable Microstructure in Dynamically Consolidated γ Titanium Aluminide. Scripta Metallurgica. 1989;23(10): 1791-1794

[26] Liu C.T., Schneibel J.H., Maziasz P.J., Wright J.L., Easton D.S.. Tensile Properties and Fracture Toughness of TiAl Alloys with Controlled Microstructures. Intermetallics. 1996;4(6):429-440

[27] Couret A., Molenat G., Galy J., Thomas M. Microstructures and Mechanical Properties of TiAl Alloy Consolidated by Spark Plasma Sintering. Intermetallics. 2008;(16): 1134-1141

[28] Liu Y.D., Liu W. Mechanical Alloying and Spark Plasma Sintering of the Intermetallic Compound $Ti_{50}Al_{50}$. Journal of Alloys and Compounds.2007;440:154-157

[29] Matsugi K., Hatayama T. Yanagisawa O. Impact Properties of Spark Sintered Titanium Aluminides at Elevated Temperatures. Intermetallics. 1999;7:1049-1057

[30] Morris M.A., Leboeuf M. Analysis of Thermal and Athermal Deformation Mechanisms during Creep of γ-TiAl Alloys. Material Science and Engineering A. 1997;239-240: 429-437

[31] Lee W.B.. Yang H.S, Kim Y.W., Mukherjee A.K. Superplastic Behavior in a Two-phase TiAl Alloy. Scripta Metallurgica et Materialia. 1993;11:1403-1408

[32] Liu Y., Lu W.J., Qin J.N., Zhang D. A New Route for the Synthesis of NdB6 powder from Nd_2O_3-B_4C System. Journal of Alloys and Compounds 2007;431:337-341

[33] Liu H.Z., Li S.E. Discussion of Metals' Resistance Temperature Coefficient. Journal of Jining Teachers College. 2001;3:12-13

[34]]Valencia J.J., McCullough C., Levi C.G., Mehrabian R. Solidification Microstructure of Supercooled Ti-Al Alloys Containing Intermetallic Phases. Acta Metallurgica. 1989;37(9):2517-2530

[35] Denquin A., Naka S. Phase Transformation Mechanisms Involved in Two-Phase TiAl-based Alloys—II. Discontinuous Coarsening and Massive-type Transformation. Acta Materialia. 1996;44(1):353-365

[36] Kumagai T., Abe E., Takeyama M., Nakamura M. Microstructural Evolution of Massively Transformed γ-TiAl during Isothermal Aging. Scripta Materialia. 1997;36(5): 523-529

[37] Li Z., Cao C. $\gamma \rightarrow \alpha$ precipitation and transformation in Ti-Al alloy. Journal of Chinese nonferrous metal. 2003;13(4):827-834

[38] Jones S.A., Kanfman M.J.. Phase Equilibria and Transformation in Intermediate Titanium-aluminum Alloys. Acta Metallurgica et Materialia. 1993;41(2):387-398

[39] Hao S., Wu W., Han C. Hisological analysisof phase transition in TiAl two-phase alloys. Acia Metallurgica Sinica. 1993;29(2):49-55

[40] Kong F., Xiao S., Chen Y., Li B. Phase transition in Ti-45Al-5Nb(-0.3Y) in the process of continous cooling. Rare metals and engineering. 2009;38(1):25-28

[41] Chen X.Q., Huang B.Y., He Y.H., Qu X.H., Lei C.H. Microstructure Characteristics of a High Ductility γ-TiAl Alloy. Acta Metallurgica Sinica. 1997;7:683-689

[42] Venkateswara K.T., Kim Y.W., Muhlstein C.L., Ritchie R.O. Fatigue-crack Growth and Fracture Resistance of a Two-phase (γ+α_2) TiAl Alloy in Duplex and Lamellar Microstructures. Materials Science and Engineering A. 1995;192-193:474-482

[43] Tang J.C., Huang B.Y., He Y.H., Liu W.S., Zhou K.C., Wu A.H. Hall-petch Relationship in Two-phase TiAl Alloys with Fully Lamellar Microstructures. Materials Research Bulletin. 2002;37:1315-1321

[44] Bohn R., Klassen T., Bormann R. Room Temperature Mechanical Behavior of Silicon-doped TiAl Alloys with Grain Size in the Nano- and Submicron-Range. Acta Materialia. 2001;49:299-311

[45] Inui H., Oh M.H., Nakamura A., Yamaguchi M.. Room-temperature Tensile Deformation of Polysynthetically Twinned (PST) Crystals of TiAl. Acta Metallurgica et Materialia. 1992;40:3095-3104

[46] Liu J., She Z.G. in: Powder Metallurgy and Ceramic Forming Technology. Chemical Industry Publishing House. 2005;116

[47] Wang J.N., Y. W. An Investigation of the Origin of the Superplasticity of Cast TiAl Alloys. International Journal of Plasticity. 2006;22(8):1530-1548

[48] Lin D.L., Sun F. Superplasticity in a Large-grained TiAl Alloy. Intermetallics. 2004;12(7-9):875-883

[49] Hsiung L.M., Nieh T.G. Microstructures and Properties of Powder Metallurgy TiAl Alloys. Materials Science and Engineering A. 2004;364(1-2):1-10

[50] Mishra R.S., Stolyarov V.V., Echer C., Valiev R.Z., Mukherjee A.K. Mechanical Behavior and Superplasticity of a Severe Plastic Deformation Processed Nanocrystalline Ti-6Al-4V Alloy. Materials Science and Engineering A. 2001;298(1-2):44-50

[51] Bohn R., lassen T.K., Bormann R. Mechanical Behavior of Submicron-Grained γ-TiAl-based Alloys at Elevated Temperatures. Intermetallics. 2001; (9):559-569

[52] Nieh T.G., Wang J.N., Lsiung L M., Wadsworth J., Sikka V. Low Temperature Superplasticity in a TiAl Alloy with a Metastable Microstructure. Scripta Materialia. 1997;37:773-779

IntechOpen